

3DMambaComplete: Exploring Structured State Space Model for Point Cloud Completion

Yixuan Li
Shanghai Key Laboratory of Data
Science, School of Computer Science,
Fudan University
Shanghai, China
yixuanli1230@gmail.com

Weidong Yang*
Shanghai Key Laboratory of Data
Science, School of Computer Science,
Fudan University
Shanghai, China
wdyang@fudan.edu.cn

Ben Fei*
Shanghai Key Laboratory of Data
Science, School of Computer Science,
Fudan University
Shanghai, China
bfei21@m.fudan.edu.cn

ABSTRACT

Point cloud completion aims to generate a complete and high-fidelity point cloud from an initially incomplete and low-quality input. A prevalent strategy involves leveraging Transformer-based models to encode global features and facilitate the reconstruction process. However, the adoption of pooling operations to obtain global feature representations often results in the loss of local details within the point cloud. Moreover, the attention mechanism inherent in Transformers introduces additional computational complexity, rendering it challenging to handle long sequences effectively. To address these issues, we propose 3DMambaComplete, a point cloud completion network built on the novel Mamba framework. It comprises three modules: HyperPoint Generation encodes point cloud features using Mamba’s selection mechanism and predicts a set of Hyperpoints. A specific offset is estimated, and the down-sampled points become HyperPoints. The HyperPoint Spread module disperses these HyperPoints across different spatial locations to avoid concentration. Finally, a deformation method transforms the 2D mesh representation of HyperPoints into a fine-grained 3D structure for point cloud reconstruction. Extensive experiments conducted on various established benchmarks demonstrate that 3DMambaComplete surpasses state-of-the-art point cloud completion methods, as confirmed by qualitative and quantitative analyses.

CCS CONCEPTS

• **Computing methodologies** → **Shape modeling; Point-based models;**

KEYWORDS

Point Cloud Completion, Structured State Space Model, Deep Learning, Mamba

1 INTRODUCTION

Point cloud, serving as a fundamental representation of three-dimensional geometry, holds significant potential in various fields such as computer graphics, robotics, and autonomous driving [5]. Acquired from LiDAR, laser scanners, or depth cameras, point clouds provide a comprehensive depiction of various properties of objects in the physical world. However, the real-world capture of point clouds often introduces various challenges, such as noise, occlusion, limitations of sensors, and reconstruction errors [7]. These factors lead to incomplete and distorted point cloud data, which unfortunately lacks crucial geometric information. Consequently,

a crucial objective in numerous applications is to reconstruct the missing parts in objects or scenes, ultimately enhancing the quality of point cloud data to support subsequent tasks [53]. Nevertheless, reconstructing point clouds presents challenges due to their disorganized, sparsity, and unstructured nature, which lacks a fixed spatial arrangement [23, 39, 45].

To address this issue, prior research has proposed to employ deep learning techniques to process point clouds, particularly emphasizing the use of 3D convolutional neural networks (3D CNNs). However, the computational demands of 3D CNN-based approaches, such as GRNet [43], have increased as the spatial resolutions have grown, thereby constraining their practical applicability. Consequently, point-based methods, pioneered by PointNet and PointNet++ [29, 30], emerged as an alternative approach, leading to the development of numerous point-based completion methods [14, 38, 41]. Inspired by the success of Transformers, recent Transformer-based approaches [3, 15, 42, 49, 57] reframed point cloud completion as a mapping problem between the partial input and complete output spaces, utilizing encoders and decoders to reconstruct the point cloud via a Transformer backbone. However, these methods still suffer from two main challenges: (i) the loss of local details due to pooling operations during encoding, and (ii) the quadratic complexity of attention mechanisms, which hinders their scalability to long sequences.

Recent advancements, such as State Space Model (SSM) [11] and Mamba [9] that use the Structured State Space Model, provide promising solutions to these challenges. Mamba, an efficient hardware perception algorithm based on Structured SSM with time-varying parameters, effectively handles long-range and sporadic data, demonstrating impressive results in 2D visual tasks [18, 59] like segmentation and classification. For the first time, PointMamba [16] extends the Mamba framework to 3D data, successfully capturing point cloud structures and showcasing its potential in 3D visual tasks. These advancements open new possibilities for developing point cloud completion methods with improved global receptive fields and linear complexity.

Drawing inspiration from the accomplishments of the Structured State Space Model, this paper aims to explore its potential in the field of point cloud completion. To address the key challenges faced by Transformer-based approaches, we introduce 3DMambaComplete, a novel point cloud completion network that first incorporates the concept of Structured State Space Model into shape reconstruction. Given input incomplete point cloud observations, 3DMambaComplete initially performs downsampling and employs EdgConv to extract feature values for the sampled points. Subsequently, the

*Corresponding author

Mamba Encoder takes the feature values of the downsampled points as input, and the Mamba Block reorders them. The data is scanned in a specific order to enhance the feature learning of the input downsampled points. Then, the Hyperpoints are predicted and refined by incorporating the downsampled points. Furthermore, by learning specific offsets, the generated Hyperpoints are dispersed across various 3D positions. Finally, 3DMambaComplete combines the downsampled points with Hyperpoints to form a novel set of hyperpoints. Notably, we devise a deliberate deformation scheme to transform the standard 2D grid of the location of each novel Hyperpoints into a cohesive 3D structure.

In summary, the contributions of 3DMambaComplete are three-fold:

- We propose 3DMambaComplete, a novel point cloud completion network based on a 3D Mamba architecture. It achieves a linear complexity and a global receptive field, effectively completing long sequences. Mamba’s selectivity enhances contextual understanding and preserves important local information for accurate reconstruction. Compactness constraint functions are designed for point generation.
- We introduce a HyperPoint Generation module to produce the new shape representation-Hyperpoints. The, while the Mamba Block enhances the sampled point features and predicts Hyperpoints. The HyperPoint Spread module disperses Hyperpoints spatially, and the Point Deformation module transforms points into a high-quality 3D structure.
- Extensive experiments demonstrate the effectiveness of 3DMambaComplete in point cloud completion. It improves reconstruction quality, especially for highly incomplete shapes, outperforming off-the-shelf methods on PCN, KITTI, and ShapeNet34/55 benchmarks.

2 RELATED WORKS

2.1 Point Cloud Completion

Point cloud completion techniques can be classified into traditional-based and deep learning-based methods. Traditional methods optimize model parameters through an optimization process to generate complete point clouds, but they are relatively slow and rely on specific geometric priors or clues [35, 55]. Deep learning-based methods have emerged as a promising solution, showing significant progress [2, 5, 20, 39]. Early attempts in this field explored the use of autoencoders [34, 38]. For instance, ASFM-Net [41], which mapped partial and complete point clouds into a shared latent space for completion. Subsequent studies incorporating the GANs [1, 52] or DDPMs [19, 58] framework have indeed yielded promising results. Zhang et al. [52] employed GAN inversion for 3D shape completion, while Luo et al. [19] utilized non-equilibrium thermodynamic diffusion processes for point cloud generation. Taking advantage of the remarkable achievements of Transformers in various domains, transformer-based methods for point cloud completion have emerged [26, 49, 50]. Xiang et al. [42] developed a snowflake-like point generation model using Skip Transformer, which mapped a 2D grid to a 3D surface and generated complete point clouds in a snowflake-like growth pattern. Point-cloud-based network structures, like PointNet [29], lack the ability to encode local features, resulting in the loss of detailed information during decoding. To

solve this, various intermediate representations such as patches, seeds, proxies, and anchors have been proposed to capture local feature information [35]. SeedFormer [57] introduces a method called “Patches Seeds” to effectively capture local information, utilizing upsampling transformers to capture spatial and semantic relationships between neighboring points. Anchorformer [3] uses pattern recognition nodes to capture regional information and combines it with sampled point and anchor information for more accurate completion. ProxyFormer [15] introduces a position encoding method that combines point cloud coordinates and features to encode partial and missing regions. However, transformer-based point cloud completion techniques [6, 8] are computationally expensive and less efficient for long sequences.

2.2 State Space Models

To enhance the long sequence modeling, State Space Models (SSMs) have arisen as a compelling solution for effectively managing long sequence data. For example, HIPPO [10] combines linear state space equations with deep learning. LSSL [12] utilizes linear state space equations and a simple neural network, achieving state-of-the-art performance on temporal sequences. Structured State Space Sequence Model (S4) [11] introduces a parameterization method for stable diagonalization, while GSS [22] reduces the dimensionality of the state space module. S5 [32] simplifies the S4 structure for practical implementation.

Nevertheless, Mamba [9] is undergoing significant development by introducing a selection mechanism and hardware-aware algorithms for efficient information processing. This breakthrough has led to further research advancements. MoE-Mamba [28] combines the Mixed Expert Model (MoE) with Mamba, enhancing state selection and improving model expressiveness and generalization. MambaByte [37] operates directly on bytes, eliminating errors and overhead from word segmentation. GraphMamba [36] extends the Sequential Symbolic Model to non-sequential graph data, improving contextual reasoning through node priorities and arrangement strategies. In biomedical imaging, Mamba also has achieved remarkable results [13, 17, 31, 48]. For instance, U-Mamba [21] enhances image segmentation accuracy and robustness, while SegMamba [44] performs segmentation on 3D images by leveraging Mamba. FDVM-Net [56] designs a frequency domain-based network for image exposure correction in endoscopic images. Vivim [47] effectively handles changes in medical videos using Mamba on video frames. However, Mamba has not been fully explored in point cloud applications [16, 54]. For the first time, this paper investigates taming Mamba for point cloud completion, which is a strength in long sequence modeling.

3 METHODS

3.1 Preliminaries

3.1.1 State Space Models. Drawing inspiration from a specific continuous system [3] and deep learning sequence models, the S4 [11] presents a proficient framework for effectively modeling Linear Time-Invariant (LTI) systems. Structured SSM achieves a sequence-to-sequence transformation $x(t) \rightarrow y(t)$ by employing a set of first-order differential equations.

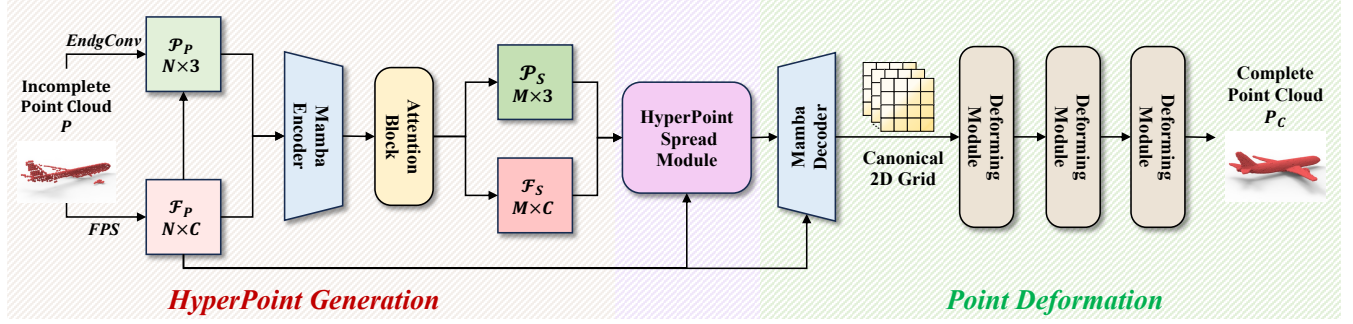


Figure 1: An overview of 3DMambaComplete. 3DMambaComplete mainly consists of three modules: (1) Given an incomplete point cloud P , mamba encoder exploits coordinates \mathcal{P}_p and features \mathcal{F}_p of the down-sampled points to generate hyperpoints \mathcal{P}_s and obtain the corresponding feature \mathcal{F}_s . (2) HyperPoint Spread Module. This module leverages enhanced features of \mathcal{P}_s and \mathcal{F}_s to broadcast hyperpoint. (3) Point Deformation. In this module, the downsampled points and hyperpoints are converted into a new set of hyperpoints using the mamba decoder. Then, a deformation module is responsible for converting the newly created hyperpoints from a 2D grid to a 3D structure.

Discretization. The first stage transforms the continuous parameters (Δ, A, B, C) to discrete parameters (\bar{A}, \bar{B}) with the discretization rule such as zero-order hold [11]. The continuous formulation is

$$\begin{aligned} \dot{h}(t) &= Ah(t) + Bx(t) \\ y(t) &= Ch(t) \end{aligned} \quad (1)$$

where $h(t)$ is an implicit latent state, $\dot{h}(t)$ denotes the time derivative of the state vector $h(t)$, and $x(t)$ is the continuous sequences. A , B and C are the parameters, and $A \in \mathbb{R}^{N \times N}$, $B \in \mathbb{R}^{N \times 1}$, $C \in \mathbb{R}^{N \times 1}$.

Computation. After the parameters have been transformed, apply a linear recursion to establish an efficient recursive relationship with respect to the hidden state h_l , the recurrence form is formulated as

$$\begin{aligned} h_l &= \bar{A}h_{l-1} + \bar{B}x_l \\ y_l &= Ch_l \end{aligned} \quad (2)$$

where $\bar{A} \in \mathbb{R}^{N \times N}$, $\bar{B} \in \mathbb{R}^{N \times 1}$.

3.1.2 Selective SSMs. To overcome the limitation of using invariant matrices Δ , A , B , and C as inputs in SSMs, which restricts the ability to effectively filter and comprehend contextual nuances across different input sequences, Gu et al. [9] introduced the S6 model, named ‘‘SSM+Selective’’. This model named Mamba, transforms SSMs from being time-invariant to time-varying by incorporating Δ , B , and C as input functions and introducing a length dimension L for the parameters. In this paper, we propose the 3DMambaComplete model, which is enhanced to capture fundamental temporal features and relationships using a selective SSMs model, an improvement that grants a more accurate and efficient representation of input sequences as a means of refining the effectiveness of point cloud complementation.

3.2 3DMambaComplete

The overview of 3DMambaComplete is depicted in Figure 1. In the following section, we describe the details of 3DMambaComplete, including HyperPoint Generation (Section 3.2.1), the HyperPoint Spread Module (Section 3.2.2), the Point Deformation Module (Section 3.2.3) and Loss Function (Section 3.2.4).

3.2.1 HyperPoint Generation. Traditional point cloud processing techniques heavily rely on pooling operations for encoding, which has resulted in a diminished capacity to capture point cloud features. On the contrary, the utilization of transformers in approaches faces a significant computational challenge as a result of its inherent second-order complexity. Therefore, this paper proposes a novel 3DMambaComplete, which exploits the advantages of structured SSM [9] and keypoint-based object-part modeling approach [3, 40]. During the learning process from input local point cloud data, 3DMambaComplete utilizes predictive modeling to identify a novel representation called hyperpoints. These hyperpoints possess distinctive features, which in turn facilitate the construction of a region recognition model. Particularly, the process of hyperpoint generation consists of two sub-blocks: the mamba Encoder and the cross-attention block.

Mamba Encoder. Given the incomplete point cloud P , we adopt Farthest Point Sampling (FPS) [29] to sample N points as $\mathcal{P}_p \in \mathbb{R}^{N \times 3}$ and extract the corresponding features $\mathcal{F}_p \in \mathbb{R}^{N \times C}$ via an EndgConv:

$$\mathcal{P}_p = \text{FPS}(P), \mathcal{F}_p = \text{EndgConv}(P, \mathcal{P}_p). \quad (3)$$

The downsampled point features \mathcal{F}_p are further transformed into a sequence of features and fed into the mamba encoder in the hyperpoint generator for enhancement. Figure 2 (left module) illustrates the details of the mamba encoder. Inspired by [27], we combine our mamba encoder along with a cross-attention block. This combination enables the generation of coordinates for the hyperpoints and enhances the features of both the generated points and the sampled points. To be more specific, the mamba encoder takes the coordinates and features of the sampled points as input. Through the mamba block, MLP layer, and residual network, it generates improved feature values for the sampled points. The mamba block utilizes layer normalization (LN), SSM, deep convolution (DW) [4], and residual connections, as shown in Figure 2 (the right module).

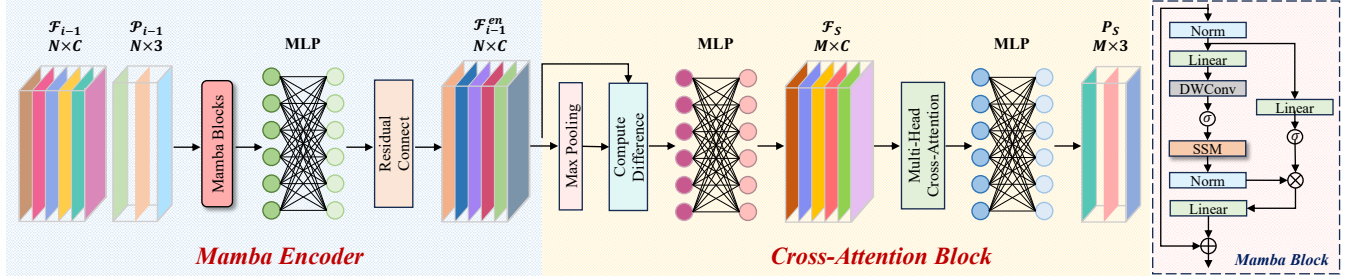


Figure 2: Details of HyperPoint Generation.

The output can be calculated by

$$\mathcal{Z}'_p = DW(MLP(LN(\mathcal{Z}_p))) \quad (4)$$

$$\mathcal{Z}''_p = MLP(LN(SSM(\sigma(\mathcal{Z}'_p)))) \quad (5)$$

$$\mathcal{Z}_p = \mathcal{Z}''_p \times \sigma(LN(\mathcal{Z}_{p-1})) + \mathcal{Z}_{p-1} \quad (6)$$

where $\mathcal{Z}_p \in \mathbb{R}^{N \times (C+3)}$ taken from the sampled point coordinates and features. The SSM is the key module in the mamba block, with a detailed description provided in Section 3.2.1. The enhanced sampled point feature values are later obtained for subsequent hyperpoint generation.

Cross-Attention Block. Figure 2 illustrates the details of the cross-attention block during the process of hyperpoint generation. In this paper, the cross-attention module is employed to predict the coordinates and features of hyperpoints. The multi-head cross-attention mechanism enables interactive processing of multiple input sequences, facilitating a better handling of the relationships between enhanced point features obtained by the Mamba Encoder. Initially, we take the enhanced point feature \mathcal{F}_{i-1}^{en} obtained from the mamba encoder as input to the cross-attention block. By applying max pooling and MLPs, we predict the features for L hyperpoints. Subsequently, we calculate the pooled feature vector h_i and the difference between h_i and \mathcal{F}_{i-1}^{en} , facilitating the representation of the enhanced features and their deviations. The hyperpoint features $\mathcal{F}_s \in \mathbb{R}^{M \times C}$ are learnt by

$$h_i = \text{MaxPool}(\mathcal{F}_{i-1}^{en}) \quad (7)$$

$$\mathcal{F}_s = \text{MLP}(h_i - \mathcal{F}_{i-1}^{en}) \quad (8)$$

where $\text{MaxPool}(\cdot)$ and $\text{MLP}(\cdot)$ are the max pooling operation and multi-layer perceptron, respectively. Moreover, we employ the multi-head cross-attention mechanism to calculate the weights between the enhanced point feature \mathcal{F}_{i-1}^{en} and the generated hyperpoint features \mathcal{F}_s , maintaining these weights for combining the input points $\mathcal{P}_{p_i} \in \mathbb{R}^{N_i \times 3}$. The resulting combination is then augmented with the pooled feature vector h_i to predict the coordinates $\mathcal{P}_{s_i} \in \mathbb{R}^{L \times 3}$ of the L hyperpoints:

$$\mathcal{P}_{s_i} = \text{MaxPool}(\text{Con}[\text{CrossAtten}(\mathcal{P}_{p_i}, \mathcal{F}_{i-1}^{en}, \mathcal{F}_s), h_i]) \quad (9)$$

where $\text{CrossAtten}(\cdot)$ and $\text{Con}(\cdot)$ serve as the multi-head cross-attention and feature concatenation. Denote all the generated L hyperpoint coordinates as \mathcal{P}_s , and the output point feature from the last cross-attention block as the feature of hyperpoints \mathcal{F}_s as \mathcal{F}_s .

3.2.2 HyperPoint Spread Module. By leveraging the Mamba encoder to generate hyperpoints, we discovered that the generated

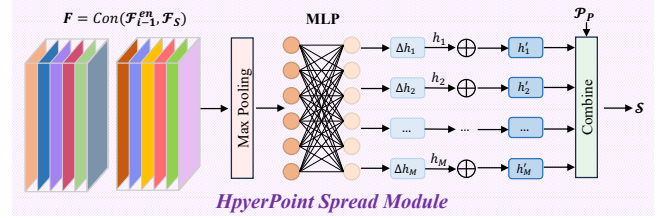


Figure 3: Detailed structure for HyperPoint Spread Module.

points exhibit a significant concentration in specific areas. To overcome this challenge, we aim to spread hyperpoints into unoccupied regions of the point cloud space. Therefore, the concept of offset is introduced to improve the accuracy of the shape reconstruction by effectively spreading the hyperpoints into the unoccupied regions of the point cloud by learning the offset.

Figure 3 vividly illustrates this spread process. The concatenation point features F acquired by the last mamba encoder and the cross-attention block of the generation module. The Max Pooling and MLP are harnessed to predict the offsets of the hyperpoints. Afterward, the attained offsets are incorporated with the hyperpoints in order to distribute each hyperpoint to a different location in 3D space, which resolves the problem of reconstruction difficulties arising from the scarcity of hyperpoints. The specific formula is as follows:

$$F = \text{Con}(\mathcal{F}_{i-1}^{en}, \mathcal{F}_s) \quad (10)$$

$$\Delta \mathcal{H} = \text{MLP}(\text{MaxPool}(F)) \quad (11)$$

$$\mathcal{H}' = \mathcal{H} + \Delta \mathcal{H}, \quad (12)$$

where $F \in \mathbb{R}^{(M+N) \times 3}$, $\Delta \mathcal{H} \in \mathbb{R}^{M \times 3}$ are the hyperpoint offsets, and \mathcal{H}' is the dispersed hyperpoints. By utilizing offset estimation, we disperse the initially missing hyperpoints into their respective regions, thereby enhancing the reconstruction of the overall 3D shape. These dispersed hyperpoints, along with the downsampled points, serve as novel hyperpoint for fine-grained 3D structure reconstruction. This approach improves the accuracy and detail of the final reconstructed point cloud.

3.2.3 Point Deformation Module. Point cloud completion methods [5] usually deform the global feature vectors from a 2D grid to a 3D structure, and lastly, gain the complete shape. However, since the global feature vectors do not take into account the 3D point-to-point relationships, the reconstructed shapes are not detailed enough. Inspired by [3, 43], we hope to incorporate local point features and the relationship between points into the reconstruction of the 3D structure, so a point deformation method is proposed to control the deformation of each hyperpoint position.

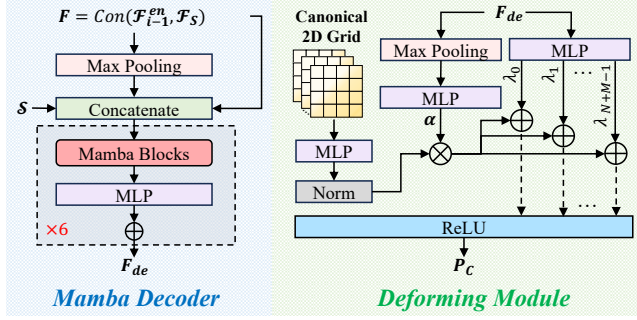


Figure 4: The pipeline of the Point Deformation.

Figure 4 portrays the structure of the two main modules in point deformation. The input consists of novel hyperpoints \mathcal{S} extracted from both the sampled points and hyperpoints, along with their corresponding features. These inputs are then passed through a mamba decoder, which is composed of 6 mamba blocks and MLP layers. The output feature F_{de} is obtained from this decoder, and subsequently, it is fed into a continuous three-layer point deformation module for local point reconstruction. The details of reconstructing points are shown in the right part of Figure 4. Specifically, we compute the outgoing feature vectors for all $N + M$ new hyperpoint, as well as the global feature vector α and the local point feature vector $\lambda \in R^{(N+M) \times C_m}$, where $\lambda = \lambda_j^{N+M-1}$. The formulas are as follows:

$$\alpha = MLP(MaxPool(F_{de})), \lambda = MLP(F_{de}), \quad (13)$$

where the output feature dimension of MLP in the m -th deforming block is C_m . Global features and local point features serve as affine parameters to reconstruct the shape for each new hyperpoint, when 2D grid features $g_{in} \in R^{K \times C_m}$ as input, the output grid feature $g_{out} \in R^{K \times C_m}$, which can be calculated by the following equation:

$$g_{out} = \lambda_j + \frac{g_{in} - \mu}{\sigma} \alpha, \quad (14)$$

where μ and σ are the mean and standard deviation of input grid feature g_{in} .

3.2.4 Loss Function. 3DMambaComplete employs an end-to-end architecture to regularize and compact the generated complete point cloud by optimizing both the reconstruction loss and the tense constraints. Firstly, the generated shape is regularized by Chamfer Distance (CD) to minimize the distance between the predicted points and the ground truth to address the common case of disordered point clouds leading to invalid loss functions. Explicitly, \mathcal{S} denotes the n_S new hyperpoints based on the predicted in 3DMambaComplete with hyperpoints and sampled points, \mathcal{P} denotes the n_P points of the completed point cloud, and \mathcal{G} denotes the ground truth, then the reconstructed point cloud loss \mathcal{L}_{rec} can be calculated as:

$$\mathcal{L}_{CD_{cg}} = \frac{1}{n_S} \sum_{c \in \mathcal{S}} \min_{g \in \mathcal{G}} \|c - g\| + \frac{1}{n_G} \sum_{g \in \mathcal{G}} \min_{c \in \mathcal{S}} \|g - c\|, \quad (15)$$

$$\mathcal{L}_{CD_{pg}} = \frac{1}{n_P} \sum_{p \in \mathcal{P}} \min_{g \in \mathcal{G}} \|p - g\| + \frac{1}{n_G} \sum_{g \in \mathcal{G}} \min_{p \in \mathcal{P}} \|g - p\|, \quad (16)$$

$$\mathcal{L}_{rec} = \mathcal{L}_{CD_{cg}} + \mathcal{L}_{CD_{pg}} \quad (17)$$

Further, we construct a minimum spanning tree on new hyperpoints using a constrained loss function such that the points in the space complemented by that point are compact. And the expansion

loss \mathcal{L}_{expan} derived from \mathcal{L}_{tree} . The functions are represented as follows:

$$\mathcal{L}_{tree}(\mathcal{P}_c, \zeta) = \sum_{(u,v) \in \mathcal{T}(\mathcal{P}_c)} \mathbb{I}\{d_{uv} \geq \zeta \eta\} d_{uv}, \quad (18)$$

$$\mathcal{L}_{expan} = \sum_{j=0}^{N+M-1} \mathcal{L}_{tree}(d_j, \varphi), \quad (19)$$

where $\mathcal{T}(\cdot)$ is the minimum spanning tree which is built on \mathcal{P}_c , and d_{uv} is the Euclidean distance between the vertex u and u in the minimum tree. \mathbb{I} is the indicator function and η is the average edge length of the minimum tree and $\mathbb{I} \cdot \zeta$ serves as a scale ratio to adjust the penalty of the distance. d_j denotes the predicted compact points around the j -th new hyperpoints.

Additionally, we add trade-off indicators τ to the tightly constrained loss function, so the final loss function can be written as:

$$\mathcal{L} = \mathcal{L}_{rec} + \tau \mathcal{L}_{expan} \quad (20)$$

4 EXPERIMENTS

In this section, we systematically test the proposed 3DMambaComplete approach extensively and compare it with several off-the-shelf techniques, including TopNet [34], PCN [51], FoldingNet [46], GRNet [43], ECG [25], CRN [38], ASFM [41], PoinTr [49], SnowflakeNet [42], ProxyFormer [15], and AnchorFormer [3]. For more information about the dataset and implementation details, please refer to the Appendix.

4.1 Experimental Metrics

For the synthetic datasets ShapeNet55/34 and PCN, we apply L_1/L_2 Chamfer Distance and F-score as evaluation metrics. The Chamfer Distance measures the average distance between the closest points of two point clouds. Given a predicted point cloud P and the ground truth G [24], Chamfer Distance is defined as:

$$CD(P, G) = \frac{1}{|P|} \sum_{p \in P} \min_{g \in G} \|p - g\| + \frac{1}{|G|} \sum_{g \in G} \min_{p \in P} \|g - p\|. \quad (21)$$

The F-score assesses the accuracy of point cloud completion with the following formula [33]:

$$F - score(\varphi) = \frac{2G(\varphi)H(\varphi)}{G(\varphi) + H(\varphi)}, \quad (22)$$

where $G(\varphi)$ and $H(\varphi)$ denote point-wise precision and recall for a threshold φ . The higher the F-score the better.

For the real-world dataset KITTI, since there is no ground truth available, we employ the minimum matching distance (MMD) and fidelity error (FD) to evaluate the effectiveness of point cloud completion. MMD measures the chamfer distance between the output and the shape of the synthetic dataset that most closely resembles the real-world input [35]. FD represents the average distance between each point in the input and its nearest neighbor in the output [5], calculating as follows:

$$FD(S_1, S_2) = \frac{1}{|S_1|} \sum_{x \in S_1} \min_{y \in S_2} \|x - y\|_2 \quad (23)$$

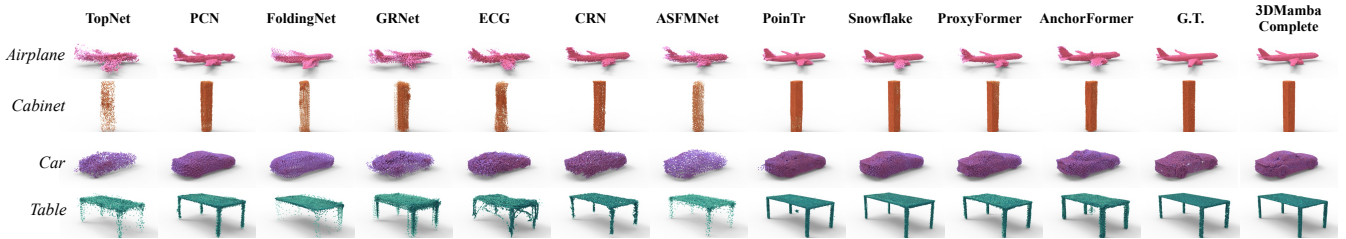


Figure 5: Visualization comparison of point cloud completion on PCN [51] dataset.

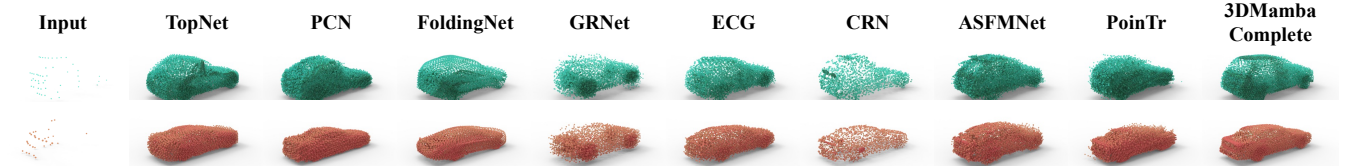


Figure 6: Visualization comparison of point cloud completion on KITTI dataset.

Table 1: Quantitative comparisons for shape completion using the ℓ_1 chamfer distance $\times 10^3$ metric on the PCN dataset with 16,384 points.

	CD- ℓ_1 ($\times 1000$)	Avg.	Airplane	Cabinet	Car	Chair	Lamp	Sofa	Table	Watercraft
TopNet [34]	15.499	9.314	17.923	13.736	17.952	17.324	18.667	15.221	13.854	
PCN [51]	11.697	6.834	12.719	9.923	13.588	13.954	14.608	11.402	10.545	
FoldingNet [46]	12.231	8.542	13.252	11.202	13.901	13.618	14.218	11.935	11.183	
GRNet [43]	12.809	8.647	14.904	11.602	14.469	13.379	15.374	13.125	10.971	
ECG [25]	10.481	6.139	13.180	9.404	10.831	10.265	13.146	12.560	8.324	
CRN [38]	12.891	7.878	15.320	12.598	13.927	13.303	16.144	12.771	11.190	
ASFM [41]	11.723	7.067	14.439	10.994	13.280	12.330	14.583	10.832	10.257	
PoinTr [49]	9.006	5.343	11.033	9.118	10.137	8.388	11.762	8.534	7.732	
SnowflakeNet [42]	8.362	5.262	10.372	8.847	9.103	7.717	10.714	7.663	7.221	
ProxyFormer [15]	11.342	6.346	12.373	9.564	13.159	13.395	14.340	11.346	10.212	
AnchorFormer [3]	7.371	3.972	9.596	8.528	8.458	6.387	9.130	6.735	6.163	
3DMambaComplete	6.907	3.861	9.115	7.721	7.412	5.733	9.042	6.288	6.085	

Table 2: Quantitative comparison on KITTI with metrics of MMD and FD.

	CD- ℓ_2 ($\times 1000$)	Fidelity	MMD	FD+MMD
TopNet [34]	1.999	0.597	2.596	
PCN [51]	1.748	0.679	2.427	
FoldingNet [46]	1.892	0.608	2.500	
GRNet [43]	0.918	0.548	1.466	
ECG [25]	0.256	0.539	0.795	
CRN [38]	2.267	1.299	3.566	
ASFM [41]	1.737	0.872	2.609	
PoinTr [49]	0.000	0.545	0.545	
3DMambaComplete	0.010	0.491	0.501	

4.2 Results on PCN Dataset

Table 1 summarizes the comparison of Chamfer Distance (CD- ℓ_1) for the eight categories in the PCN dataset. Table 1 clearly demonstrates that the 3DMambaComplete model outperforms all other baseline models, achieving the lowest chamfer distance and average value in each category. Specifically, the average CD- ℓ_1 of the 3DMambaComplete model is 6.907, which is significantly lower (2.099 lower) than the best competitor Anchorformer. In addition, Figure 5 visually presents the results obtained by 3DMambaComplete. It demonstrates the effectiveness of our model in accurately predicting missing parts of 3D objects while utilizing a reduced number of points, resulting in improved accuracy. This highlights the capability of the 3DMambaComplete model to capture essential information and incorporate contextual details through Mamba blocks. Furthermore, it illustrates the advantages of learning a set of hyperpoints for describing regional information.

4.3 Results on KITTI Dataset

After fine-tuning a pre-trained model on the PCN dataset, we further tested it on the KITTI dataset and compared it with other state-of-the-art methods, as shown in Table 2. Figure 6 presents the visual comparisons on the KITTI dataset. It is observed that when dealing with real scan data with a high degree of missing input data, 3DMambaComplete outperforms previous methods significantly. This indicates that the Hyperpoints and downsampled points generated by 3DMambaComplete accurately capture the features of the input point cloud.

4.4 Results on ShapeNet55 Dataset

Due to the exceptional performance of 3DMambaComplete on the PCN and KITTI datasets, we expanded our testing to include the ShapeNet55 dataset, which offers a larger variety of categories. The results, shown in Table 3, highlight the impressive performance of 3DMambaComplete on the ShapeNet55 dataset. Across all categories, the average CD- ℓ_1 is 13.837, the average CD- ℓ_2 is 0.862, and the average F-score@1% is 0.341. Particularly noteworthy is the improvement in completion performance as the masking ratio increases (as observed in CD-H). In this scenario, the average CD- ℓ_1 for all categories is 15.384, and the average CD- ℓ_2 is 1.194, surpassing the performance of the second-best method, AnchorFormer. Moreover, we assess the performance of 3DMambaComplete in categories with sufficient training samples (Table, Chair, Airplane, Bag, and Rocket) and categories with limited training samples (Birdhouse, Bag, Remote, Keyboard, and Rocket). Table 3 confirms that 3DMambaComplete achieves the highest CD scores in categories with sufficient training samples and maintains excellent performance even in categories with limited training samples. Other baselines, except for PointTr, struggle due to imbalanced training sample quantities, resulting in higher CD losses. Visual comparisons in Figure 7 further validate the effectiveness of 3DMambaComplete, which generates more accurate and detailed complete shapes compared to other methods across diverse environments.

4.5 Results on ShapeNet34/Unseen21 Dataset

We execute experiments on ShapeNet34 and ShapeNetUnseen21 to assess the generalization ability of 3DMambaComplete. The results,

Table 3: Quantative comparison on ShapeNet55 using $CD-\ell_2 \times 10^3$ as well as the average F-Score@1%. We employed various difficulty levels, CD-S, CD-M, and CD-H, to evaluate the completion results that represent *Simple*, *Moderate*, and *Hard* settings, respectively.

	F1-Avg	CD-S	CD-M	CD-H	CD-Avg	Table	Chair	Airplane	Car	Sofa	Bridhouse	Bag	Remote	Keyboard	Rocket
		($CD-\ell_1/CD-\ell_2$)	($CD-\ell_1/CD-\ell_2$)	($CD-\ell_1/CD-\ell_2$)	($CD-\ell_1/CD-\ell_2$)	(F-Score-Avg/ /CD- ℓ_1 -Avg/ /CD- ℓ_2 -Avg)	(F-Score-Avg/ /CD- ℓ_1 -Avg/ /CD- ℓ_2 -Avg)	(F-Score-Avg/ /CD- ℓ_1 -Avg/ /CD- ℓ_2 -Avg)	(F-Score-Avg/ /CD- ℓ_1 -Avg/ /CD- ℓ_2 -Avg)	(F-Score-Avg/ /CD- ℓ_1 -Avg/ /CD- ℓ_2 -Avg)	(F-Score-Avg/ /CD- ℓ_1 -Avg/ /CD- ℓ_2 -Avg)	(F-Score-Avg/ /CD- ℓ_1 -Avg/ /CD- ℓ_2 -Avg)	(F-Score-Avg/ /CD- ℓ_1 -Avg/ /CD- ℓ_2 -Avg)	(F-Score-Avg/ /CD- ℓ_1 -Avg/ /CD- ℓ_2 -Avg)	(F-Score-Avg/ /CD- ℓ_1 -Avg/ /CD- ℓ_2 -Avg)
TopNet [34]	0.11	27.233 2.483	28.749 2.848	33.986 4.642	29.989 3.324	0.147 25.106 2.438	0.088 29.754 2.950	0.203 20.034 1.397	0.077 27.212 2.089	0.077 28.739 2.449	0.046 38.762 4.899	0.084 30.489 2.998	0.121 25.026 1.982	0.218 18.306 1.091	0.278 19.874 1.498
PCN [51]	0.167	22.990 1.811	23.976 2.062	27.360 2.937	24.775 2.270	0.181 21.694 1.812	0.143 24.558 2.084	0.340 16.428 0.985	0.103 23.398 1.531	0.101 24.364 1.765	0.062 34.575 4.022	0.127 26.025 2.293	0.228 18.418 1.042	0.272 16.272 0.924	0.343 18.590 1.318
FoldingNet [46]	0.091	25.203 2.095	26.596 2.410	30.424 3.33	27.407 2.612	0.163 23.298 1.953	0.066 27.193 2.350	0.172 19.749 1.331	0.063 25.383 1.777	0.061 26.753 2.076	0.027 36.924 4.291	0.066 27.559 2.439	0.139 20.136 1.209	0.201 18.123 1.054	0.209 19.423 1.260
GRNet [43]	0.239	19.157 1.137	20.647 1.489	24.037 2.394	21.280 1.673	0.231 19.397 1.355	0.412 21.213 1.575	0.150 14.830 0.830	0.150 21.931 1.351	0.150 22.026 1.435	0.135 27.352 7.735	0.210 22.028 1.691	0.306 17.277 0.953	0.293 15.678 0.783	0.536 13.596 0.855
ECG [25]	0.321	16.709 1.167	18.726 1.545	23.478 2.555	19.638 1.756	0.320 17.912 1.543	0.336 18.233 1.409	0.559 12.347 0.657	0.255 18.161 1.033	0.234 19.813 1.421	0.194 25.926 2.830	0.285 20.013 1.677	0.374 15.865 0.961	0.454 12.887 0.688	0.639 11.742 0.701
CRN [38]	0.205	21.207 1.502	22.364 1.801	25.849 2.726	23.140 2.010	0.214 20.313 1.570	0.183 22.931 1.859	0.357 15.231 0.842	0.118 23.804 1.606	0.142 23.367 1.663	0.102 32.237 3.599	0.163 24.139 2.040	0.247 18.163 1.041	0.266 15.767 0.815	0.485 14.522 0.930
ASFM-Net [41]	0.247	19.136 1.307	20.170 1.517	23.512 2.282	20.940 1.702	0.294 17.788 1.241	0.209 21.216 1.595	0.426 14.242 0.748	0.164 21.076 1.293	0.177 20.875 1.371	0.122 27.936 2.769	0.219 21.092 1.618	0.332 16.140 0.880	0.358 14.256 0.677	0.522 9.894 0.867
PoinTr [49]	0.446	12.491 0.698	14.181 1.049	18.812 2.022	15.161 1.256	0.480 13.041 0.979	0.438 14.838 1.149	0.598 10.137 0.547	0.368 15.747 0.974	0.394 14.790 1.790	0.348 20.670 2.131	0.416 15.295 1.179	0.467 13.722 0.992	0.533 10.159 0.452	0.693 9.842 0.627
Snowflake [42]	0.343	14.596 0.817	16.644 1.175	21.545 2.207	17.595 1.406	0.373 15.194 1.053	0.345 16.918 1.267	0.497 12.394 0.677	0.222 18.571 1.181	0.295 16.902 1.053	0.233 22.415 2.162	0.336 17.401 1.325	0.426 13.618 0.714	0.456 11.602 0.494	0.611 11.684 0.722
ProxyFormer [15]	0.175	22.382 1.751	23.315 2.000	26.975 3.053	24.224 2.268	0.195 21.321 1.934	0.156 23.549 2.003	0.346 16.181 0.978	0.096 24.002 1.630	0.127 22.993 1.682	0.070 33.334 3.837	0.137 24.283 2.121	0.230 18.064 1.037	0.255 16.167 0.906	0.433 16.341 1.137
AnchorFormer [3]	0.327	15.391 1.138	15.555 1.124	18.351 1.913	16.432 1.392	0.372 14.040 0.989	0.324 15.768 1.164	0.510 10.969 0.548	0.190 18.145 1.158	0.276 15.971 1.021	0.189 22.742 2.523	0.315 15.599 1.118	0.434 12.167 0.591	0.434 11.109 0.592	0.629 10.543 0.642
3DMambaComplete	0.341	12.698 0.617	13.431 0.775	15.384 1.194	13.837 0.862	0.326 13.489 0.854	0.299 14.781 0.972	0.513 10.033 0.468	0.166 17.150 1.029	0.240 15.347 0.894	0.177 20.798 1.934	0.280 14.815 0.946	0.389 11.723 0.552	0.375 10.612 0.416	0.649 9.627 0.551

Table 4: The quantitative comparison on ShapeNet34 and ShapeNetUnseen21 using $CD-\ell_1/CD-\ell_2 \times 10^3$, as well as the average F-Score@1%.

	ShapeNet34					ShapeNetUnseen21				
	CD-S ($CD-\ell_1/CD-\ell_2$)	CD-M ($CD-\ell_1/CD-\ell_2$)	CD-H ($CD-\ell_1/CD-\ell_2$)	CD-Avg ($CD-\ell_1/CD-\ell_2$)	F1-Avg	CD-S ($CD-\ell_1/CD-\ell_2$)	CD-M ($CD-\ell_1/CD-\ell_2$)	CD-H ($CD-\ell_1/CD-\ell_2$)	CD-Avg ($CD-\ell_1/CD-\ell_2$)	F1-Avg
TopNet [34]	22.382/1.606	23.271/1.793	26.020/2.432	23.891/1.944	0.154	26.775/2.499	28.312/2.928	33.121/4.407	29.403/3.278	0.103
PCN [51]	21.433/1.551	22.304/1.753	25.086/2.426	22.941/1.910	0.192	27.593/2.983	28.988/3.442	34.598/5.558	30.393/3.994	0.128
FoldingNet [46]	23.556/1.859	24.466/2.059	28.584/2.759	25.535/2.226	0.137	28.356/2.887	29.832/3.290	35.356/4.968	31.181/3.715	0.088
GRNet [43]	18.809/1.102	20.032/1.365	22.990/2.090	20.610/1.519	0.247	21.247/1.554	23.757/2.287	29.426/4.169	24.810/2.670	0.208
ECG [25]	13.123/0.735	14.627/0.996	18.459/1.696	15.403/1.142	0.496	15.283/1.255	17.596/1.759	23.534/3.267	18.804/2.094	0.460
CRN [38]	20.304/1.362	21.216/1.594	24.159/2.318	21.893/1.758	0.221	24.247/2.237	26.076/2.840	31.771/4.833	27.365/3.303	0.177
ASFM-Net [41]	18.351/1.189	19.123/1.342	21.914/1.909	19.796/1.480	0.268	21.591/1.995	23.007/2.342	27.629/3.660	24.076/2.666	0.216
PoinTr [49]	12.006/0.632	13.393/0.910	17.364/1.697	14.254/1.080	0.459	13.289/0.838	15.521/1.376	21.881/3.070	16.897/1.761	0.421
SnowflakeNet [42]	13.966/0.714	15.613/0.987	19.646/1.730	16.408/1.144	0.362	15.639/1.055	18.157/1.558	24.338/3.151	19.378/1.921	0.324
ProxyFormer [15]	21.463/1.637	22.226/1.827	25.114/2.591	22.934/2.018	0.198	26.954/3.065	28.313/3.516	33.716/5.530	29.660/4.037	0.139
AnchorFormer [3]	14.662/0.853	15.504/1.087	18.096/1.770	16.087/1.237	0.328	16.017/1.097	17.543/1.582	21.811/2.887	18.457/1.855	0.289
3DMambaComplete	13.247/0.661	14.056/0.844	16.385/1.391	14.563/0.965	0.324	14.560/0.859	21.173/2.990	16.225/1.343	17.319/1.731	0.281

presented in Table 4, demonstrate that 3DMambaComplete performs better on seen categories compared to unseen categories. Notably, under the *hard* masking setting, 3DMambaComplete achieves the lowest $CD-\ell_1$ and $CD-\ell_2$ on both the 34 seen categories and the 21 unseen categories, showcasing its exceptional completion capability for severely incomplete point cloud shapes. While ECG achieves the best F-score@1%, its $CD-\ell_1$ and $CD-\ell_2$ are relatively higher, and the visual results are not as satisfactory as those of our 3DMambaComplete, as shown in Figure 8. The figure illustrates

visually appealing completions for the 21 unseen categories, demonstrating the excellent generalization ability of 3DMambaComplete to previously unseen objects.

5 ABLATION STUDY

Ablation Study on the Number of Mamba Layers. To demonstrate the effectiveness of 3DMambaComplete, we conducted a comprehensive study on the reduction of Mamba block layers. As shown in Table 5, we selected 1, 3, 6, 9, and 12 different Mamba

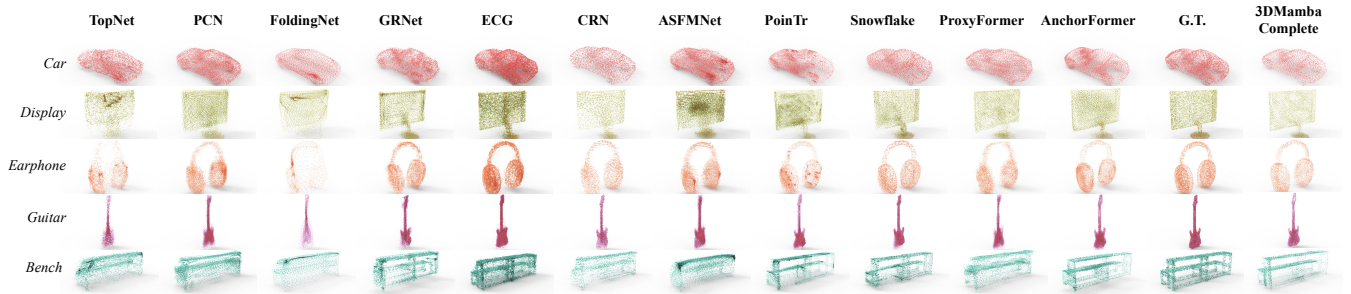


Figure 7: Visualization comparison of point cloud completion on ShapeNet55 [49] dataset.

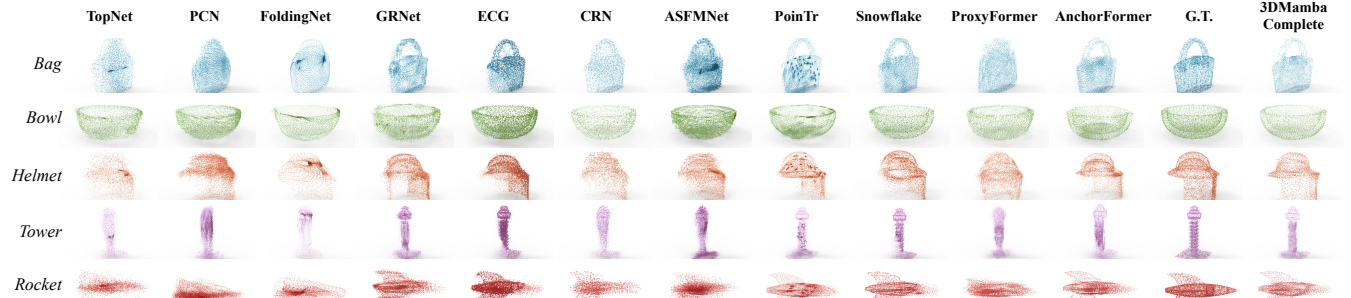


Figure 8: Visualization comparison of point cloud completion on ShapeNetUnseen21 [49] dataset.

Table 5: The ablation study on the number of mamba layers. All the models are tested on PCN dataset [51].

Number of Mamba Layer	CD- ℓ_1	CD- ℓ_2	F-score@1%
1	7.284	0.220	0.796
3	7.044	0.204	0.810
6(Ours)	6.907	0.207	0.824
9	7.054	0.203	0.809
12	7.120	0.209	0.805

Table 6: Performance comparisons among different variants of 3DMambaComplete on the PCN dataset [51].

Model	Mamba Block	HyperPoint	Deformation	\mathcal{L}_{expn}	CD- ℓ_1	CD- ℓ_2	F-Score
I	MLP	✓	✓	✓	8.095	0.238	0.727
II	Transformer	✓	✓	✓	7.352	0.216	0.790
III	✓	Global Feature	✓	✓	7.410	0.218	0.786
IV	✓	✓	Folding	✓	7.716	0.222	0.763
V	✓	✓	✓	-	7.302	0.213	0.798
Ours	✓	✓	✓	✓	6.907	0.207	0.824

block layers for comparison. The results indicate that 3DMambaComplete performs the best among its peers when the number of Mamba layers is 6. We thought that a smaller number of Mamba blocks may result in inadequate extraction of local point cloud information, while a larger number of Mamba blocks not only increases computational costs but also fails to effectively capture key information within the Mamba structure.

Ablation Study on the Different Variants. We undertake relevant ablation experiments to examine several novel aspects of 3DMambaComplete, as shown in Table 6. In the Mamba Block Module, we compare MLP (Model I) and Transformer (Model II) designs, both of which underperform compared to the Mamba structure. In the HyperPoint Module, using only Global Feature (Model III) for reconstruction leads to inferior results compared to 3DMambaComplete. Additionally, experiments in the Point Deformation Module

Table 7: Complexity analysis. The number of parameters (Params) and theoretical computation cost (FLOPs) of existing methods are reported.

Methods	Param.	FLOPs
ASFM-Net [41]	10.76 M	7.15 G
FoldingNet [46]	2.30 M	25.81 G
PCN [51]	6.55 M	13.71 G
TopNet [34]	5.76 M	6.72 G
GRNet [43]	73.15 M	17.55 G
ECG [25]	13.77 M	9.32 G
CRN [38]	5.00 M	14.40 G
SnowflakeNet [42]	18.43 M	5.20 G
PoinTr [49]	87.14 M	10.41 G
ProxyFormer [15]	19.64 M	4.67 G
AnchorFormer [3]	29.05 M	7.60 G
Ours	34.06 M	7.12 G

(Model IV) and Loss Function (Model V) highlight the importance of point transformation and expansion loss for effective point cloud reconstruction in 3DMambaComplete.

Ablation Study on the Complexity analysis. Furthermore, we evaluated the Param. and FLOPs of different methods. As a result of incorporating downsampled points and generated hyperpoints as inputs for the final Point Deformation, 3DMambaComplete exhibits a slightly higher number of parameters and increased FLOPs compared to ProxyFormer [15]. However, visualizations indicate that 3DMambaComplete achieves superior reconstruction results for partial point clouds, suggesting that the utilization of downsampled points contributes to the effectiveness of point cloud reconstruction.

6 CONCLUSION

This paper introduces a novel point cloud completion technique called 3DMambaComplete based on the brand-new Mamba framework. This method utilizes pattern-aware discriminative nodes,

known as Hyperpoints, to dynamically capture regional information of objects. It leverages Mamba’s selectivity to enhance the connectivity between local and global contexts of the point cloud, thereby improving the quality of the reconstructed point cloud. To demonstrate the effectiveness of this approach, we compare 3DMambaComplete with state-of-the-art point cloud completion methods. The evaluation results indicate that 3DMambaComplete successfully captures point cloud information and reconstructs complete point clouds with fine-grained details, outperforming these existing methods.

REFERENCES

- [1] Panos Achlioptas, Olga Diamanti, Ioannis Mitliagkas, and Leonidas Guibas. 2018. Learning representations and generative models for 3d point clouds. In *International conference on machine learning*. PMLR, 40–49.
- [2] Yingjie Cai, Kwan-Yee Lin, Chao Zhang, Qiang Wang, Xiaogang Wang, and Hongsheng Li. 2022. Learning a structured latent space for unsupervised point cloud completion. In *Proceedings of the IEEE/CVF conference on computer vision and pattern recognition*. 5543–5553.
- [3] Zhikai Chen, Fuchen Long, Zhaofan Qiu, Ting Yao, Wengang Zhou, Jiebo Luo, and Tao Mei. 2023. AnchorFormer: Point Cloud Completion From Discriminative Nodes. In *Proceedings of the IEEE/CVF Conference on Computer Vision and Pattern Recognition*. 13581–13590.
- [4] François Chollet. 2017. Xception: Deep learning with depthwise separable convolutions. In *Proceedings of the IEEE conference on computer vision and pattern recognition*. 1251–1258.
- [5] Ben Fei, Weidong Yang, Wen-Ming Chen, Zhijun Li, Yikang Li, Tao Ma, Xing Hu, and Lipeng Ma. 2022. Comprehensive review of deep learning-based 3d point cloud completion processing and analysis. *IEEE Transactions on Intelligent Transportation Systems* 23, 12 (2022), 22862–22883.
- [6] Ben Fei, Weidong Yang, Wen-Ming Chen, and Lipeng Ma. 2022. VQ-DcTr: Vector-quantized autoencoder with dual-channel transformer points splitting for 3D point cloud completion. In *Proceedings of the 30th ACM international conference on multimedia*. 4769–4778.
- [7] Ben Fei, Weidong Yang, Lipeng Ma, and Wen-Ming Chen. 2023. DcTr: Noise-robust point cloud completion by dual-channel transformer with cross-attention. *Pattern Recognition* 133 (2023), 109051.
- [8] Ben Fei, Rui Zhang, Weidong Yang, Zhijun Li, and Wen-Ming Chen. 2024. Progressive Growth for Point Cloud Completion by Surface-Projection Optimization. *IEEE Transactions on Intelligent Vehicles* (2024).
- [9] Albert Gu and Tri Dao. 2023. Mamba: Linear-time sequence modeling with selective state spaces. *arXiv preprint arXiv:2312.00752* (2023).
- [10] Albert Gu, Tri Dao, Stefano Ermon, Atri Rudra, and Christopher Ré. 2020. Hippo: Recurrent memory with optimal polynomial projections. *Advances in neural information processing systems* 33 (2020), 1474–1487.
- [11] Albert Gu, Karan Goel, and Christopher Ré. 2021. Efficiently modeling long sequences with structured state spaces. *arXiv preprint arXiv:2111.00396* (2021).
- [12] Albert Gu, Isys Johnson, Karan Goel, Khaled Saab, Tri Dao, Atri Rudra, and Christopher Ré. 2021. Combining recurrent, convolutional, and continuous-time models with linear state space layers. *Advances in neural information processing systems* 34 (2021), 572–585.
- [13] Tao Guo, Yinuo Wang, and Cai Meng. 2024. Mambamorph: a mamba-based backbone with contrastive feature learning for deformable mr-ct registration. *arXiv preprint arXiv:2401.13934* (2024).
- [14] Zitian Huang, Yikuan Yu, Jiawen Xu, Feng Ni, and Xinyi Le. 2020. Pf-net: Point fractal network for 3d point cloud completion. In *Proceedings of the IEEE/CVF conference on computer vision and pattern recognition*. 7662–7670.
- [15] Shanshan Li, Pan Gao, Xiaoyang Tan, and Mingqiang Wei. 2023. ProxyFormer: Proxy Alignment Assisted Point Cloud Completion with Missing Part Sensitive Transformer. In *Proceedings of the IEEE/CVF Conference on Computer Vision and Pattern Recognition*. 9466–9475.
- [16] Dingkan Liang, Xin Zhou, Xinyu Wang, Xingkui Zhu, Wei Xu, Zhikang Zou, Xiaoqing Ye, and Xiang Bai. 2024. PointMamba: A Simple State Space Model for Point Cloud Analysis. *arXiv preprint arXiv:2402.10739* (2024).
- [17] Jiarun Liu, Hao Yang, Hong-Yu Zhou, Yan Xi, Lequan Yu, Yizhou Yu, Yong Liang, Guangming Shi, Shaoting Zhang, Hairong Zheng, et al. 2024. Swin-mamba: Mamba-based unet with imagenet-based pretraining. *arXiv preprint arXiv:2402.03302* (2024).
- [18] Yue Liu, Yunjie Tian, Yuzhong Zhao, Hongtian Yu, Lingxi Xie, Yaowei Wang, Qixiang Ye, and Yunfan Liu. 2024. Vmamba: Visual state space model. *arXiv preprint arXiv:2401.10166* (2024).
- [19] Shitong Luo and Wei Hu. 2021. Diffusion probabilistic models for 3d point cloud generation. In *Proceedings of the IEEE/CVF Conference on Computer Vision and Pattern Recognition*. 2837–2845.
- [20] Zhaoyang Lyu, Zhifeng Kong, Xudong Xu, Liang Pan, and Dahua Lin. 2021. A conditional point diffusion-refinement paradigm for 3d point cloud completion. *arXiv preprint arXiv:2112.03530* (2021).
- [21] Jun Ma, Feifei Li, and Bo Wang. 2024. U-mamba: Enhancing long-range dependency for biomedical image segmentation. *arXiv preprint arXiv:2401.04722* (2024).
- [22] Harsh Mehta, Ankit Gupta, Ashok Cutkosky, and Behnam Neyshabur. 2022. Long range language modeling via gated state spaces. *arXiv preprint arXiv:2206.13947* (2022).
- [23] Paritosh Mittal, Yen-Chi Cheng, Maneesh Singh, and Shubham Tulsiani. 2022. Autosdf: Shape priors for 3d completion, reconstruction and generation. In *Proceedings of the IEEE/CVF Conference on Computer Vision and Pattern Recognition*. 306–315.
- [24] Trung Nguyen, Quang-Hieu Pham, Tam Le, Tung Pham, Nhat Ho, and Binh-Son Hua. 2021. Point-set distances for learning representations of 3d point clouds. In *Proceedings of the IEEE/CVF international conference on computer vision*. 10478–10487.
- [25] Liang Pan. 2020. ECG: Edge-aware point cloud completion with graph convolution. *IEEE Robotics and Automation Letters* 5, 3 (2020), 4392–4398.
- [26] Yatian Pang, Wenxiao Wang, Francis EH Tay, Wei Liu, Yonghong Tian, and Li Yuan. 2022. Masked autoencoders for point cloud self-supervised learning. In *European conference on computer vision*. Springer, 604–621.
- [27] Jonathan Pilault, Mahan Fathi, Orhan Firat, Chris Pal, Pierre-Luc Bacon, and Ross Goroshin. 2024. Block-state transformers. *Advances in Neural Information Processing Systems* 36 (2024).
- [28] Maciej Pióro, Kamil Ciebiera, Krystian Król, Jan Ludziejewski, and Sebastian Jaszczur. 2024. Moe-mamba: Efficient selective state space models with mixture of experts. *arXiv preprint arXiv:2401.04081* (2024).
- [29] Charles R Qi, Hao Su, Kaichun Mo, and Leonidas J Guibas. 2017. Pointnet: Deep learning on point sets for 3d classification and segmentation. In *Proceedings of the IEEE conference on computer vision and pattern recognition*. 652–660.
- [30] Charles Ruizhongtai Qi, Li Yi, Hao Su, and Leonidas J Guibas. 2017. Pointnet++: Deep hierarchical feature learning on point sets in a metric space. *Advances in neural information processing systems* 30 (2017).
- [31] Jiacheng Ruan and Suncheng Xiang. 2024. Vm-unet: Vision mamba unet for medical image segmentation. *arXiv preprint arXiv:2402.02491* (2024).
- [32] Jimmy TH Smith, Andrew Warrington, and Scott W Linderman. 2022. Simplified state space layers for sequence modeling. *arXiv preprint arXiv:2208.04933* (2022).
- [33] Marina Sokolova, Nathalie Japkowicz, and Stan Szpakowicz. 2006. Beyond accuracy, F-score and ROC: a family of discriminant measures for performance evaluation. In *Australasian joint conference on artificial intelligence*. Springer, 1015–1021.
- [34] Lyne P Tchappmi, Vineet Kosaraju, Hamid Rezatofighi, Ian Reid, and Silvio Savarese. 2019. Topnet: Structural point cloud decoder. In *Proceedings of the IEEE/CVF conference on computer vision and pattern recognition*. 383–392.
- [35] Keneni W Tesema, Lyndon Hill, Mark W Jones, Muneeb I Ahmad, and Gary KL Tam. 2023. Point Cloud Completion: A Survey. *IEEE Transactions on Visualization and Computer Graphics* (2023).
- [36] Chloe Wang, Oleksii Tsepa, Jun Ma, and Bo Wang. 2024. Graph-mamba: Towards long-range graph sequence modeling with selective state spaces. *arXiv preprint arXiv:2402.00789* (2024).
- [37] Junxiang Wang, Tushaar Gankavrapu, Jing Nathan Yan, and Alexander M Rush. 2024. Mambabyte: Token-free selective state space model. *arXiv preprint arXiv:2401.13660* (2024).
- [38] Xiaogang Wang, Marcelo H Ang Jr, and Gim Hee Lee. 2020. Cascaded refinement network for point cloud completion. In *Proceedings of the IEEE/CVF conference on computer vision and pattern recognition*. 790–799.
- [39] Yida Wang, David Joseph Tan, Nassir Navab, and Federico Tombari. 2022. Learning local displacements for point cloud completion. In *Proceedings of the IEEE/CVF conference on computer vision and pattern recognition*. 1568–1577.
- [40] Weikun Wu, Yan Zhang, David Wang, and Yunqi Lei. 2020. SK-Net: Deep learning on point cloud via end-to-end discovery of spatial keypoints. In *Proceedings of the AAAI Conference on Artificial Intelligence*, Vol. 34. 6422–6429.
- [41] Yaqi Xia, Yan Xia, Wei Li, Rui Song, Kailang Cao, and Uwe Stilla. 2021. Asfnet: Asymmetrical siamese feature matching network for point completion. In *Proceedings of the 29th ACM international conference on multimedia*. 1938–1947.
- [42] Peng Xiang, Xin Wen, Yu-Shen Liu, Yan-Pei Cao, Pengfei Wan, Wen Zheng, and Zhizhong Han. 2021. Snowflakenet: Point cloud completion by snowflake point deconvolution with skip-transformer. In *Proceedings of the IEEE/CVF international conference on computer vision*. 5499–5509.
- [43] Haozhe Xie, Hongxun Yao, Shangchen Zhou, Jiageng Mao, Shengping Zhang, and Wenxiu Sun. 2020. Grnet: Gridding residual network for dense point cloud completion. In *European Conference on Computer Vision*. Springer, 365–381.
- [44] Zhaohu Xing, Tian Ye, Yijun Yang, Guang Liu, and Lei Zhu. 2024. Segmamba: Long-range sequential modeling mamba for 3d medical image segmentation. *arXiv preprint arXiv:2401.13560* (2024).

- [45] Xingguang Yan, Liqiang Lin, Niloy J Mitra, Dani Lischinski, Daniel Cohen-Or, and Hui Huang. 2022. Shapeformer: Transformer-based shape completion via sparse representation. In *Proceedings of the IEEE/CVF Conference on Computer Vision and Pattern Recognition*. 6239–6249.
- [46] Yaoqing Yang, Chen Feng, Yiru Shen, and Dong Tian. 2018. Foldingnet: Point cloud auto-encoder via deep grid deformation. In *Proceedings of the IEEE conference on computer vision and pattern recognition*. 206–215.
- [47] Yijun Yang, Zhaohu Xing, and Lei Zhu. 2024. Vivim: a video vision mamba for medical video object segmentation. *arXiv preprint arXiv:2401.14168* (2024).
- [48] Zi Ye and Tianxiang Chen. 2024. P-Mamba: Marrying Perona Malik Diffusion with Mamba for Efficient Pediatric Echocardiographic Left Ventricular Segmentation. *arXiv preprint arXiv:2402.08506* (2024).
- [49] Xumin Yu, Yongming Rao, Ziyi Wang, Zuyan Liu, Jiwen Lu, and Jie Zhou. 2021. PointR: Diverse point cloud completion with geometry-aware transformers. In *Proceedings of the IEEE/CVF international conference on computer vision*. 12498–12507.
- [50] Xumin Yu, Lulu Tang, Yongming Rao, Tiejun Huang, Jie Zhou, and Jiwen Lu. 2022. Point-bert: Pre-training 3d point cloud transformers with masked point modeling. In *Proceedings of the IEEE/CVF conference on computer vision and pattern recognition*. 19313–19322.
- [51] Wentao Yuan, Tejas Khot, David Held, Christoph Mertz, and Martial Hebert. 2018. Pcn: Point completion network. In *2018 international conference on 3D vision (3DV)*. IEEE, 728–737.
- [52] Junzhe Zhang, Xinyi Chen, Zhongang Cai, Liang Pan, Haiyu Zhao, Shuai Yi, Chai Kiat Ye, Bo Dai, and Chen Change Loy. 2021. Unsupervised 3d shape completion through gan inversion. In *Proceedings of the IEEE/CVF Conference on Computer Vision and Pattern Recognition*. 1768–1777.
- [53] Rui Zhang, Jingyi Xu, Weidong Yang, Lipeng Ma, Menglong Chen, and Ben Fei. 2024. Learning Density Regulated and Multi-View Consistent Unsigned Distance Fields. In *ICASSP 2024-2024 IEEE International Conference on Acoustics, Speech and Signal Processing (ICASSP)*. IEEE, 8366–8370.
- [54] Tao Zhang, Xiangtai Li, Haobo Yuan, Shunping Ji, and Shuicheng Yan. 2024. Point Cloud Mamba: Point Cloud Learning via State Space Model. *arXiv preprint arXiv:2403.00762* (2024).
- [55] Xuancheng Zhang, Yutong Feng, Siqi Li, Changqing Zou, Hai Wan, Xibin Zhao, Yandong Guo, and Yue Gao. 2021. View-guided point cloud completion. In *Proceedings of the IEEE/CVF conference on computer vision and pattern recognition*. 15890–15899.
- [56] Zhuoran Zheng and Jun Zhang. 2024. FD-Vision Mamba for Endoscopic Exposure Correction. *arXiv preprint arXiv:2402.06378* (2024).
- [57] Haoran Zhou, Yun Cao, Wenqing Chu, Junwei Zhu, Tong Lu, Ying Tai, and Chengjie Wang. 2022. Seedformer: Patch seeds based point cloud completion with upsampling transformer. In *European conference on computer vision*. Springer, 416–432.
- [58] Linqi Zhou, Yilun Du, and Jiajun Wu. 2021. 3d shape generation and completion through point-voxel diffusion. In *Proceedings of the IEEE/CVF international conference on computer vision*. 5826–5835.
- [59] Lianghai Zhu, Bencheng Liao, Qian Zhang, Xinlong Wang, Wenyu Liu, and Xinggang Wang. 2024. Vision mamba: Efficient visual representation learning with bidirectional state space model. *arXiv preprint arXiv:2401.09417* (2024).